Regimes of Boiling

1.1 Introduction

Boiling heat transfer is defined as a mode of heat transfer that occurs with a change in phase from liquid to vapor. Depending upon its mobility it has been classified in two categories (i) Pool Boiling, (ii) Flow or convective Boiling. Pool boiling occurs in relatively quiescent fluids where as later occurs in flowing stream of fluid.

1.2 Regimes of Boiling

Various regimes in a typical case of pool boiling in water at atmospheric pressure are shown in Figure 1.1, which is conventionally the log-log representation of heat versus wall superheat. In the range *A-B,* the water is heated by natural convection. With the mechanism of single-phase natural convection, the heat transfer rate *q"* is proportional to $\Delta T_{sat}^{5/4}$. In the range B-C, the liquid near the wall is superheated and tend to evaporate, forming bubbles. The mechanism in this range is called nucleate boiling. There are two subregimes in nucleate boiling: local boiling and bulk boiling. Local boiling is the nucleate boiling in a subcooled liquid, where the bubbles formed at the heating surface and tend to condense locally. Bulk boiling is nucleate in a saturated liquid; in this case, the bubbles do not collapse. In the nucleate boiling range, q" varies as ΔT^{n}_{sat}, where n generally ranges from 2 to 5. When the population of bubbles becomes too high at some high heat flux point C, the outgoing bubbles may obstruct the path of the incoming fluid. The vapor thus forms an insulating blanket covering the heating surface and thereby raises the surface temperature. This is called as boiling crisis or burnout or DNB (Departure from Nucleate Boiling). In the range C-D, immediately after the critical heat flux has been reached, boiling becomes unstable and the mechanism is then called partial film boiling or transition boiling. The surface is alternately covered with a vapor blanket and a liquid layer, resulting in oscillating surface temperatures. If the power input to the heater is maintained, the surface temperature increases rapidly to reach the point D while the heat flux steadily decreases. In the range D-E, a stable vapor film is formed on the heating surface and the heat transfer rate reaches a minimum. This is called stable film boiling. By further increasing the wall temperature, the heat transfer rate also is increased by thermal radiation.

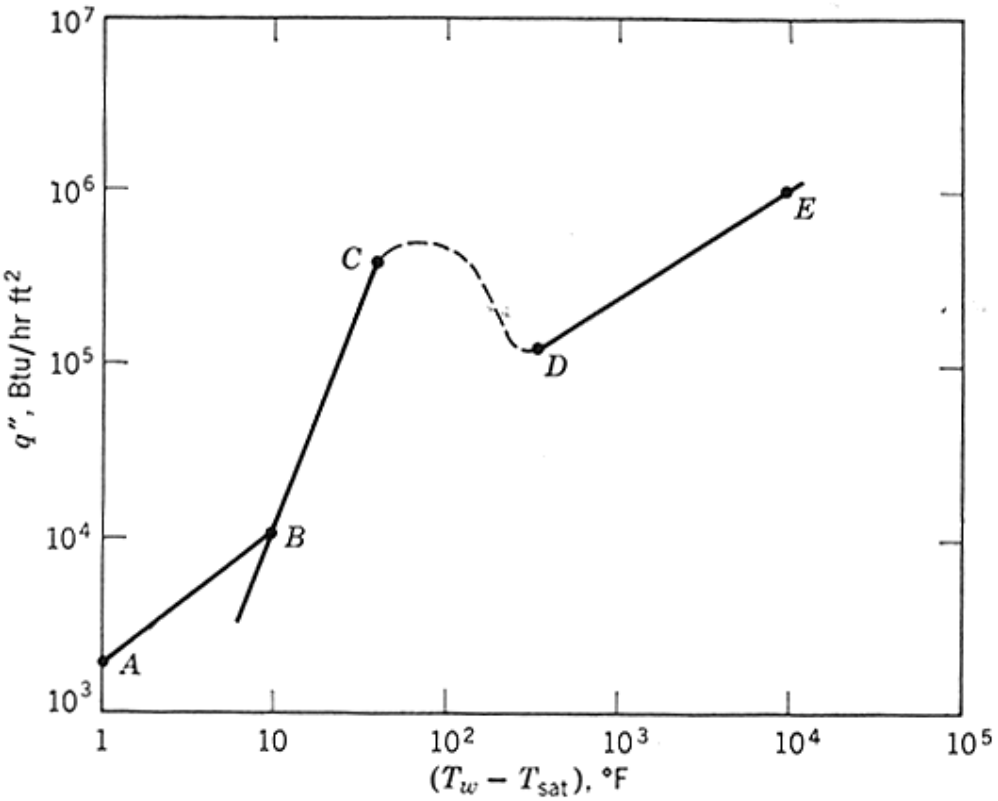

Fig. 1.1 Pool boiling regimes. A-B, natural convection; B-C, nucleate boiling; C-D, partial film boiling; D-E, stable film boiling [26].

In flow boiling, the boiling regimes mentioned above also exist. The mechanisms are more complicated, however, owing to the fact that the two-phase flow plays an important role in the boiling process. For instance, the flow shear may cut off the bubbles from the wall so that the average bubble size is reduced and the frequency is increased.

Pool Boiling and Flow Boiling

2.1 Pool Boiling

In pool boiling fluid motion is initiated and maintained by nucleation, growth departure, collapse of bubbles and also by natural convection. But in macroscopic level it remains stationary i.e. flow is not present.

2.2 Nucleation in a pure liquid

Nucleation is a process, on a molecular scale, in which a small bubble (nucleus) of size just in excess of the thermodynamic equilibrium is formed. Inertia and surface tension effects control initial growth from the nucleation size. The primary requirement for nucleation to occur or for a nucleus to subsist in a liquid is that the liquid be superheated. Volmer [1] established an expression for the rate of nucleation in a superheated liquid:

$$\frac{dn}{dt} = NBe^{(H_{fg}/KT + w_o/KT)} \tag{2.1}$$

Where n is the number of nuclei

N is the total number of molecules in a system

B is a function of b, where b is the pressure ratio,

$$b = \frac{p_v - p_l}{p_l}$$

H_{fg} is the heat of evaporation per molecule, in Btu/molecule

K is the gas constant per molecule

T is the temperature in ^oR

w_o is the work of creating the free surface of a nucleus, in ft-lb, given by Volmer as

$$w_o = (4\pi r^2\sigma - v\Delta p) = \frac{16\pi\sigma^3}{3(p_v - p_l)^2}$$

The condition for thermodynamic equilibrium at a vapor-liquid interface in a pure substance can be written as

$$P_v - P_l = \sigma(\frac{1}{R_1} + \frac{1}{R_2}) \tag{2.2}$$

where R_1 and R_2 are the principal radii of curvature of the interface. For a spherical nucleus of radius R, equation (2.2) becomes

$$P_v - P_l = \frac{2\sigma}{R} \tag{2.3}$$

For a bulk liquid at pressure P_l, the vapor pressure P_v of the super heated liquid near the wall can be related to the amount of superheat, $T_v - T_{sat}$, by the Clausius –Clapeyron equation

$$\frac{dp}{dT} = \frac{H_{fg} J}{v_{fg} T} \tag{2.4}$$

which, in finite difference form and $v_v >> v_l$, becomes

$$P_v - P_l = (T_v - T_{sat}) \frac{H_{fg} J \rho_v}{T_{sat}} \tag{2.5}$$

Combining equations (2.3) and (2.5) yields for the equilibrium bubble size

$$R = \frac{2\sigma}{J H_{fg} \rho_v} \frac{T_{sat}}{(T_v - T_{sat})} \tag{2.6}$$

Hence, for increasing superheat, the nucleation size can be smaller, and by equation (2.1) the number of nuclei formed per unit time increases. Another implication of equation (2.6) is that only a nucleus of the equilibrium size is stable. A smaller nucleus will collapse, and a larger nucleus will grow.

2.3 Nucleation at surfaces

The number of potential nucleation sites is usually observed by photographic inspection of the heater surface. Gaertner [2] has reported that, from a cursory examination of published data for liquids boiling from three different surfaces, the population of active sites was found to be

$$\bar{N} = N_o \exp(-\frac{K}{T_{wall}^3}) \tag{2.7}$$

where N_o and K represent the liquid and surface conditions. It was stated by Gaertner that at present it is still not possible to predict N_o and K for a particular boiling system. However, it can be seen that the population of active sites is a strong function of wall temperature and thereby of heat flux.

Air dispersed in small bubbles or entrapped in surface crevices markedly decreases the degree of liquid superheat attained at a solid liquid interface. The required superheat for

nucleation is reduced when small amounts of permanent gas are present in dispersion or trapped on surfaces can readily be demonstrated. The equation of thermodynamic equilibrium of a spherical gas-vapor bubble (nucleus) becomes

$$P_g + P_v - P_l = \frac{2\sigma}{R} \tag{2.8}$$

where the partial pressure of the permanent gas, P_g, can be related to the total mass of gas, w_g, in the bubble by the ideal gas law as

$$P_g = \frac{3w_g KT_v}{4\pi R^3} \tag{2.9}$$

Combining equations (2.8) and (2.9) gives

$$P_v - P_l = \frac{2\sigma}{R} - \frac{3w_g KT_v}{4\pi R^3} \tag{2.10}$$

Equation (2.10) may be combined with equation (2.5) to evaluate the required superheat for a given nucleus.

In another approach, Ellion [3] defines a critical radius for which a nucleus containing w_g lb of gas will be stable. At the critical radius it requires a maximum superheat. If the superheat is not enough, the bubble will stop growing. The value of the critical radius can be obtained from equation (2.10) by setting

$$\frac{\partial(P_v - P_l)}{\partial R} = 0$$

Then

$$R_{crit} = 3\left(\frac{w_g KT_v}{8\pi\sigma}\right)^{1/2}$$

and, substituting into equation (2.10), we get

$$(P_v - P_l)_{crit} = \frac{4}{9}\sigma\left(\frac{8\pi\sigma}{w_g KT_v}\right)^{1/2}$$

or

$$R_{crit} = \frac{4\sigma}{3(P_v - P_l)_{crit}} \tag{2.11}$$

A gas-vapor nucleus greater than the critical size will grow indefinitely

2.4 Isothermal Bubble Dynamics

When the size of a bubble nucleus formed in a liquid exceeds that of thermodynamic equilibrium given by equation (2.3), the bubble will grow because of the excess vapor pressure that is no longer balanced by the surface tension forces. During the

initial stage of the growth, the inertia of the surrounding liquid and the surface forces control the process. Considering a single spherical bubble in an incompressible inviscous liquid of infinite extent, the equation of motion for the spherically symmetrical domain of the liquid is

$$\rho_l(\frac{\partial u}{\partial t}+u\frac{\partial u}{\partial r})=-\frac{\partial p}{\partial r} \tag{2.12}$$

Integrating the equation of continuity

$$\frac{1}{r^2}\frac{\partial}{\partial r}(r^2u)=0 \tag{2.13}$$

from the radius of bubble interface R to r, where r > R, gives the radial liquid velocity u in terms of the interface velocity:

$$\dot{R}=\frac{dR}{dt}$$

$$u=\dot{R}(\frac{R}{r})^2 \tag{2.14}$$

Substituting equation (2.14) into equation (2.12) gives

$$\rho_l\left[\frac{2R\dot{R}^2+R^2\ddot{R}}{r^2}-\frac{2\dot{R}R^4}{r^5}\right]=-\frac{\partial p}{\partial r} \tag{2.15}$$

which, upon integration from the bubble interface to infinity, gives

$$\rho_l\left(R\ddot{R}+\frac{3}{2}\dot{R}^2\right)=P_l(R)-P_l(\infty) \tag{2.16}$$

The vapor pressure in the bubble is related to the liquid pressure at the bubble interface and the surface tension force by equation (2.3). Introducing this result into equation (2.16), the Rayleigh equation for isothermal bubble dynamics is obtained as

$$\rho_l\left(R\ddot{R}+\frac{3}{2}\dot{R}^2\right)=\Delta p-\frac{2\sigma}{R} \tag{2.17}$$

where $\Delta P = P_v - P_l(\infty)$ can again be related to the liquid superheat by the Clausius-Clapeyron equation to give the initial value of the driving pressure difference for bubble growth. The initial bubble size, which to facilitate growth must exceed the critical size given by equation (2.3), is generally not known. Idealized models are therefore postulated to describe bubble growth, using equation (2.17).

2.5 Correlation of Pool Boiling Crisis Data

Boiling crisis is a sudden drop of heat transfer coefficient occurring after a very high heat flux in nucleate boiling has been reached. This sudden drop of heat transfer coefficient will cause a surface temperature surge which usually melts the heating surface, if the power to it is maintained constant. This phenomenon is, therefore, also called burnout.

The physical description of boiling crisis in pool boiling is that, when the heat flux and liquid superheat increase, the active nucleation sites become so numerous that the bubbles at the surface coalesce to form a blanketing layer of vapor.

Rohsenow and Griffith [4] obtained a correlation of the critical flux:

$$\frac{q''}{H_{fg}\rho_v} = 143\left(\frac{\rho_l - \rho_v}{\rho_v}\right)^{0.6} g^{1/4} \tag{2.18}$$

Zuber [5] postulated that boiling crisis is due to Helmholtz instability. He correlated q"$_{out}$ with the critical vapor velocity from equation as

$$\frac{q''_{crit}}{H_{fg}\rho_v} = \frac{\pi}{16}V_v \tag{2.19}$$

The result may be written as

$$\frac{q''_{crit}}{H_{fg}\rho_v} = \frac{\pi}{24}\left[\frac{\sigma(\rho_l - \rho_v)g}{\rho_v^2}\right]^{1/4}\left[\frac{\rho_l}{\rho_l + \rho_v}\right]^{1/2} \tag{2.20}$$

Addoms [6] has suggested a correlation for pool boiling crisis: as

$$q''_{crit} = 2.4H_{fg}\rho_v\left[\frac{\rho_l - \rho_v}{\rho_v}\right]^{1/2}\left[\frac{k}{\rho c}\right]_l^{1/2} \tag{2.21}$$

Chang and Snyder [7] have used wave motion theory and suggested a correlation for predicting the pool boiling critical heat flux:

$$q''_{crit} = \frac{\pi}{12}H_{fg}\rho_v^{1/4}\left[\frac{\rho_l + \rho_v}{\rho_l}\right]^{1/2}\left[g\sigma(\rho_l - \rho_v)\right]^{1/4} \tag{2.22}$$

Kutateladze [8] has developed a critical heat flux correlation in saturated pool boiling by using dimensional analysis. The dimensionless groups considered are

$$\frac{V_v^2}{Lg},\quad \frac{\rho_v}{\rho_l - \rho_v},\quad \frac{q''}{H_{fg}\rho_v V_v},\quad \frac{g\Delta P}{\rho_v V_v^2},\quad \frac{\sigma}{\Delta P L}$$

By combining these groups in the following manner:

$$\frac{V_v^2}{Lg} * \frac{\rho_v}{\rho_l - \rho_v} * \left(\frac{q^{"}}{H_{gf} \rho_v V_v} \right)^2 * \left[\frac{g(\rho_l - \rho_v) L^2}{\sigma} \right]^{0.5} = K$$

the following correlation is obtained:

$$q^{"}_{crit} = \sqrt{K} \left[H_{fg} \sqrt{\rho_v} \sqrt[4]{\sigma(\rho_l - \rho_v) g} \right] \tag{2.23}$$

Kutateladze's experimental data indicate that the average value of $\sqrt{K}$ is 0.14, obtained from a range from 0.13 to 0.19 for various surface conditions of horizontal wires and disks.

To extend the validity of this correlation to subcooled liquids, a heat conduction term was added by Zuber et al.[9] to account for the intermittent contact of subcooled fluid and heating surface. The following ratio results:

$$\frac{q_{crit,subcooled}}{q_{crit,saturated}} = 1 + \frac{5.3}{H_{fg} \rho_v} \sqrt{k_l \rho_l c_p} * \left[\frac{g(\rho_l - \rho_v)}{\sigma} \right]^{1/4} \left[\frac{\sigma g (\rho_l - \rho_v)}{\rho_v^2} \right]^{-1/8} (T_{sat} - T_b) \tag{2.24}$$

This equation agrees with the critical flux in pool boiling of subcooled water and ethyl alcohol at less than 142 psia, according to Kutateladze and Schneiderman [10].

Ivey and Morris [11] reported the ratio of subcooled critical flux to saturated critical flux of pool boiling in water, ethyl alcohol, ammonia, carbon tetrachloride, and isooctane for pressures from 4.5 to 500 psia as

$$\frac{q^{"}_{crit,sub}}{q_{crit,sat}} = 1 + 0.1 \left(\frac{\rho_v}{\rho_l} \right)^{1/4} \left[\frac{c_p \rho_l (T_w - T_b)}{H_{fg} \rho_v} \right] \tag{2.25}$$

2.6 Effects of Parameters on Pool Boiling Crisis

In the following paragraphs the influences on the critical heat flux in pool boiling of a number of experimental parameters are examined.

2.6.1 ***The effect of Surface Tension.*** The effect of surface tension in the Kutateladze equation is represented as $q^{"}_{crit} \sim \sigma^{1/4}$. However Adams [12] found that, on vertical heaters 2 to 4 in. long, $q^{"}_{crit} \sim \sigma$.

2.6.2 ***Effect of Agitation.*** The critical heat flux of pool boiling can be increased considerably by introducing agitation. Pramuk and Westwater [13] as shown in Figure 2.1 obtained experimental evidence.

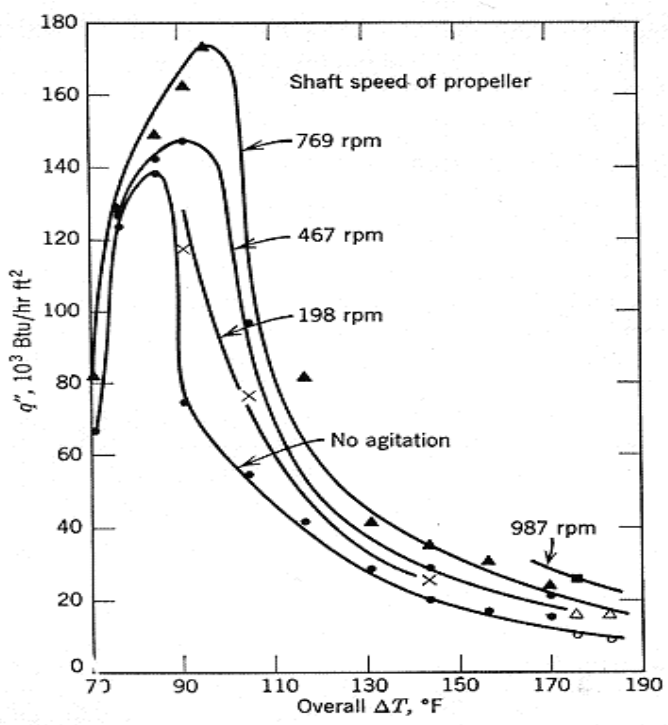

Fig 2.1 Effect of Agitation in methanol boiling at 1 atm [26].

2.6.3 ***Effect of Acceleration.*** The effect of acceleration implied in equation (2.23) is that $q''_{crit} \sim (a/g)^{0.25}$. However, by employing graphite heaters operating in pure distilled water, Adams [12], has found

$q''_{crit} \sim (a/g)^{0.15}$ for 0 < a/g < 10

$q''_{crit} \sim (a/g)^{0.25}$ for 10 < a/g < 100

2.6.4 ***Effect of Surface Conditions.*** Berenson [14] studied the effects of a wetting agent and surface conditions on critical heat flux in pool boiling. His data were obtained from an upward-facing surface of a metallic block; they are reproduced in Figure 2.2. His conclusions are:

1. The maximum heat flux is practically independent of surface material, cleanliness, and roughness (emery 320, 60, lap, or mirror finish).
2. A smooth surface has a larger (T_w - T_{sat}) at boiling crisis than a rough surface, although bith have approximately the same critical flux.
3. The transition boiling heat transfer rate is increased by a dirty surface and the presence of a wetting agent (oleic acid).
4. The minimum film boiling flux is independent of surface material, cleanliness, and roughness provided that the roughness height in less than the film thickness.

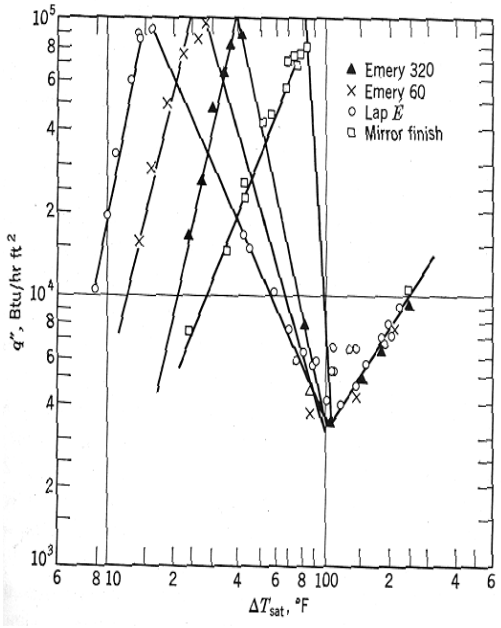

Fig 2.2 Copper-pentane test results: effects of roughness[26].

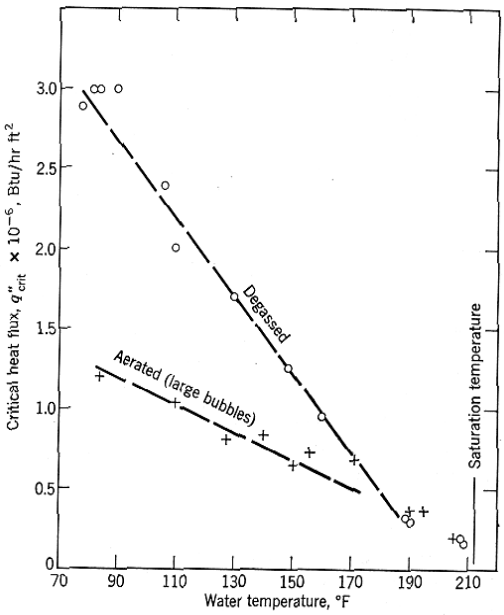

Fig 2.3 Effect of dissolved gas and subcooling on CHF under atm. Pressure[26].

Ivey and Morris [15] stated that oxidized surfaces appear to yield a higher critical heat flux than that associated with clean metallic surfaces.

2.6.5 ***Effect of Diameter and Orientation of Heater.*** Von Stralen [16] has found that, with a fixed system pressure, a reduction of bubble size (accomplished by small additions of volatile organic liquids to the water) resulted in raising the peak heat flux to more than twice its original value for small heater diameters and to the "asymptotic" value for large heater diameters. Costello and Frea [17] have reported that, for semicylindrical heat transfer surfaces of small diameters (less than 0.5 in.), significant increase in critical heat flux can be obtained by depositing a surface coating such as that obtained from tap water. Less effect was observed for a heater of large diameter.

2.6.7 ***Effect of Gases and Volatile (Binary Mixture).*** Noncondensable gases dissolved in water produce a premature boiling crisis. Figure 2.3 is a graph of data from Ellion [3] which describe the effects of dissolved gas and subcooling on the critical flux under pool boiling conditions. Yang [18] reported that the nucleate boiling heat transfer of a heat transfer of a binary mixture increases as Jakob number of each component decreases.

2.7 Flow Boiling

Flow boiling is distinguished from pool boiling by the presence of fluid flow caused by natural circulation in a loop or forced by an external pump. Beyond critical heat flux, an unstable region of heat transfer termed partial film boiling or transition

boiling occurs. This is gradually converted to stable film boiling as the surface temperature increases above the Leidenfrost point.

2.8 The Regimes of Heat Transfer

Consider a vertical tube uniformly heated over its length with a low heat flux and fed with subcooled liquid at its base at such a rate that the liquid is totally evaporated over the length of the tube. Figure 2.4 shows, in diagrammatic form, the various flow patterns encounterd over the length of the tube, together with the corresponding heat transfer regions.

While the liquid is being heated up to the saturation temperature and the wall temperature remains below that necessary for nucleation, the process of heat transfer is single-phase convective heat transfer to the liquid phase (region A). At some point along the tube, the conditions adjacent to the wall are such that the formation of vapor from nucleation sites can occur. Initially vapor formation takes place in the presence of subcooled liquid (region B) and this heat transfer mechanism is known as subcooled nucleate boiling. In the subcooled boiling region, B, the wall temperature remains essentially constant a few degrees above saturation temperature, whilst the mean bulk fluid temperature is increasing to the saturation temperature. The amount by which the wall temperature exceeds the saturation temperature is known as the 'degree of superheat', ΔT_{sat}, and the difference between the saturation and local bulk fluid temperature is known as the 'degree of subcooling', ΔT_{sub}.

The transition between regions B and C, the subcooled nucleate boiling region and the saturated nucleate boiling is clearly defined from thermodynamic viewpoint. It is point at which liquid reaches the saturation temperature (x = 0) found on the basis of simple heat balance calculations. However, subcooled liquid can persist in the liquid in the liquid core even in the region defined as saturated nucleate boiling. Vapor generated in the subcooled region is present at the transition between regions B and C (x = 0); thus some of the liquid must be subcooled to ensure that the liquid mixed mean (mixing cup) enthalpy equals that of saturated liquid (i_f). This effect occurs as a result of the radial temperature profile in the liquid and subcooled liquid flowing in the center of channel will only reach the saturation temperature at some distance downstream of the point x = 0.

In the regions C to G, the variable characterizing the heat transfer mechanism is the thermodynamic mass 'quality' (x) of the fluid. Let the enthalpy of the liquid at the tube

inlet be i_{fi} (corresponding to a temperature T_{fi}). Then the enthalpy after a length, z, along the tube is given by

$$i(z) = i_{fi} + \frac{4\phi z}{DG} \tag{2.26}$$

The 'quality' of the vapor-liquid mixture at a distance, z is given on a thermodynamic basis as

$$x(z) = \frac{i(z) - i_f}{i_{fg}} \tag{2.27}$$

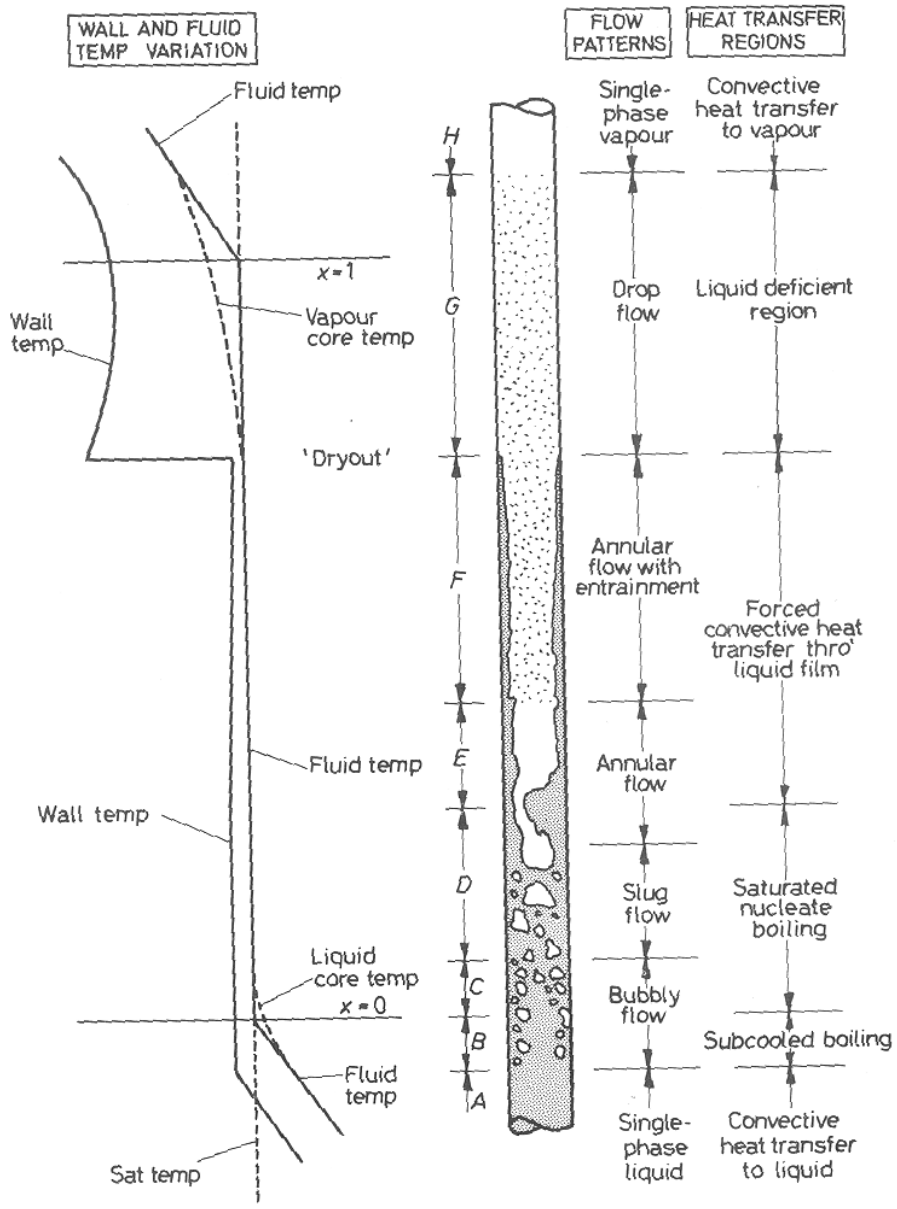

Fig 2.4 Regions of Heat Transfer in Convective Boiling [30].

or in terms of heat flux and length

$$x(z) = \frac{4\phi}{DGi_{fg}}(z - z_{SC}) \tag{2.28}$$

where z_{SC} is the length of tube required to bring the enthalpy of the liquid up to the saturated liquid enthalpy, i_f. In the region $0 < x < 1$ and for complete thermodynamic equilibrium, *x* represents the ration of the vapor mass flow rate to the total mass flow rate. As the quality increases through the saturated nucleate boiling region a point may be reached where a fundamental transition in mechanism of heat transfer takes place. The process of 'evaporation' replaces the process of 'boiling'. This transition is preceded by a change in the flow pattern from bubbly or slug flow to annular flow (regions E and F). In the latter regions the thickness of the thin liquid film on the heating surface is often such that the effective thermal conductivity is sufficient to prevent the liquid in contact with the wall being superheated to a temperature which would allow bubble nucleation. Heat is carried away from the wall by forced convection in the film to the liquid film-vapor core interface, where evaporation occurs. Since the nucleation is completely suppressed, the heat transfer process can no longer be called 'boiling'. The region beyond the transition has been referred to as the two-phase forced convective region of heat transfer (regions E and F).

At some critical value of the quality the complete evaporation of liquid film occurs. This transition is known as 'dryout' and is accompanied by a rise in the wall temperature for channels operating with a controlled surface heat flux. The area between the dryout point and the transition to dry saturated vapor (region H) has been termed the liquid deficient region (corresponding to the drop flow pattern)(region G). This condition of dryout often puts an effective limit on the amount of evaporation that can be allowed to take place in a tube at a particular value of heat flux.

Critical heat flux in forced convective flow

3.1 Introduction

The critical heat flux condition is characterized by a sharp reduction of the local heat transfer coefficient which results from the replacement of liquid by vapor adjacent to the heat transfer surface.

When the bulk fluid is at the subcooled at the location where the critical heat flux is exceeded, the critical condition is termed 'DNB' (subcooled) – departure from subcooled nucleate boiling. Similarly, where saturated nucleate boiling occurs just prior to the critical condition, the term is 'DNB' (saturated) – departure from saturated nucleate boiling. For higher fluid enthalpies where nucleation is suppressed and where the flow pattern is likely to be annular, the term 'dryout' is used to imply that drying out of the liquid film is the cause of the critical heat flux condition. Practically all of the experimental studies of the onset of critical heat flux condition have been carried out using heated surfaces for which the heat flux rather than the surface temperature is independently controlled. Considerable differences are also found to exist in the practical methods used to define and measure the critical condition.

3.2 CHF for Forced Convective Flow of Water in Circular Conduits with Uniform Heat Flux

3.2.1 *Some initial Considerations*

In general, for uniformly heated channels, it can be assumed that the onset of the critical heat flux condition occurs first at the exit end of the channel. For non-uniform axial heat flux distribution, over heating may occur first at the exit or upstream of exit.

The critical heat flux condition cannot exist if the heater surfaces temperature lies below the saturation temperature. Thus the minimum possible critical heat flux is given by

$$(\phi_{crit})_{\min} = \frac{(\Delta T_{sub})_i}{\left[4z/\left(Gc_{pf}D\right)+1/h_{fo}\right]} \tag{3.1}$$

The critical heat flux condition must occur at or before all the liquid fed to the channel is evaporated (x(z) = 1) leading to

$$\left(\phi_{crit}\right)_{\max} = \frac{GDi_{fg}}{4z}\left[1+\frac{c_{pf}\left(\Delta T_{sub}\right)_i}{i_{fg}}\right] \tag{3.2}$$

The possible range of conditions for the critical heat flux can be shown diagrammatically (Figure 3.1). These limits are derived from very simple self-evident consideration but when correlations are applied to any particular problem it is prudent to check that the estimated critical heat flux does, in fact, lie within the specified limits particularly if the values of the independent variables are outside the range covered by the original correlation.

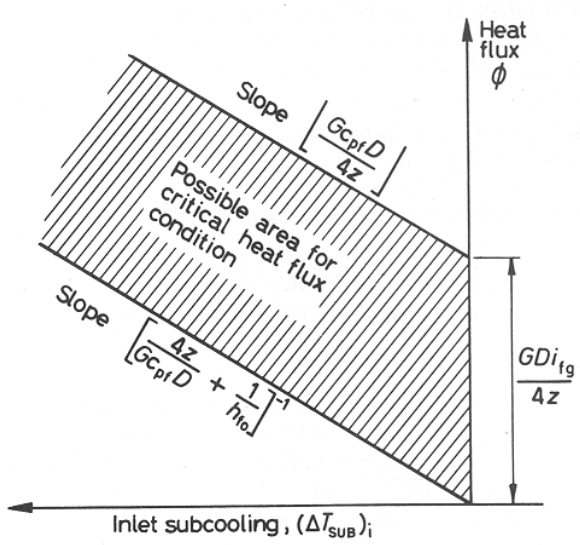

Fig 3.1 Defining the Limits of the Critical Heat Flux Condition [30].

3.2.2 *General Relationships between Independent Variables and Methods of Display of Experimental Data*

Earlier it was postulated that the critical heat flux for water in a vertical uniformly heated tube is a function of five independent variables, thus,

$$\phi_{crit} = fn(G, (\Delta T_{sub})_i, p, D, z) \tag{3.3}$$

Since overheating of the tube surface at the critical condition almost invariably begins at the exit of the heated section, it can be argued that display and correlation should be terms of exit conditions. Either the fluid enthalpy i(z) or the thermodynamic mass quality x(z) may be chosen to characterize the exit conditions. Each of these dependent variable is related to the inlet subcooling via the heat balance equation thus,

$$i(z) = i_f + \frac{4\phi z}{Dg} - (\Delta T_{sub})_i c_{pf} \tag{3.4}$$

$$x(z) = \frac{1}{i_{fg}}\left[\frac{4\phi z}{DG} - (\Delta T_{sub})_i c_{pf}\right] \tag{3.5}$$

Thus, as alternatives to equation (3.3) it is possible to write

$$\phi_{crit} = fn(G, i(z), p, D, z) \tag{3.6}$$

$$\phi_{crit} = fn(G, x(z), p, D, z) \tag{3.7}$$

The tube may be divided into two lengths; over the first length (z_{sc}) the liquid is raised to the saturation condition ($x(z_{sc}) = 0$) and over the second length (z_{sat}) the quality is raised from zero to $x(z)$ the outlet quality corresponding to the critical condition. The following relationships hold:

$$z = z_{sc} + z_{sat} \tag{3.8}$$

$$z_{sc} = \frac{DG(\Delta i_{sub})_i}{4\phi_{crit}} \tag{3.9}$$

$$z_{sat} = \frac{x(z)DGi_{fg}}{4\phi_{crit}} \tag{3.10}$$

For a fixed $x(z)$ and ϕ_{crit}, the value of z_{sat} is also fixed, though z_{sc} will vary with subcooling. This implies that the only function of z_{sc} is to heat the fluid up to the saturation condition at the appropriate flux. With the assumed relationship

$$\phi_{crit} = fn(x(z), G, p, D) \tag{3.11}$$

it follows from the above equation that these further equations hold:

$$\phi_{crit} = fn(z_{sat}, G, p, D) \tag{3.12}$$

$$x_{crit} = fn(z_{sat}, G, p, D) \tag{3.13}$$

Equation (3.11) suggests there is a local relationship between critical heat flux and quality whereas equation (3.13) suggests that the mass fraction of the liquid which can be evaporated (x_{crit}) in the channel before the onset of the critical condition is a function of the length over which the evaporation takes place, (z_{sat}). Neither of these two views of the critical heat flux phenomenon is completely correct and neither, as it turns out, can be used as a general basis for the prediction of more complex cases.

The relationship between ϕ_{crit}, $(\Delta T_{sub})_i$ and D. the effect of tube diameter on the relationship between ϕ_{crit} and $(\Delta i_{sub})_i$ and between ϕ_{crit} and x(z) for fixed values of G, z, and p can be well illustrated by plotting the data of Lee and Obertelli [19]. These data were obtained for a pressure of 69 bar, a mass velocity of 2000 kg/m^2 s and for tube lengths in the range 1.93-2 m.

Figure 3.2 shows the critical heat flux plotted against inlet subcooling for six tube diameter ranging from 5.58 mm to 37.45 mm. As the tube diameters is increased, so the

critical heat flux increases at constant inlet subccoling. The relationship between critical heat flux and inlet subcooling is linear for small tube diameters ($D \leq 12.8$ mm) but the larger diameters show a marked curvature. Figure 3.3 shows the same data plotted against exit quality. Where the data for different tube diameters overlap, it can be seen that the critical heat flux decreases with increasing tube diameter for a given exit quality.

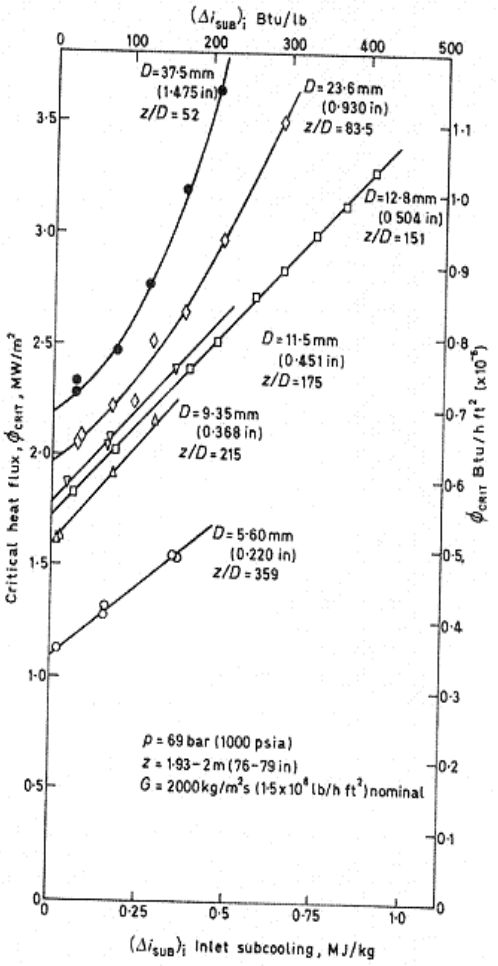

Fig 3.2 The influence of Tube Diameter on CHF at Fixed Inlet Conditions [30].

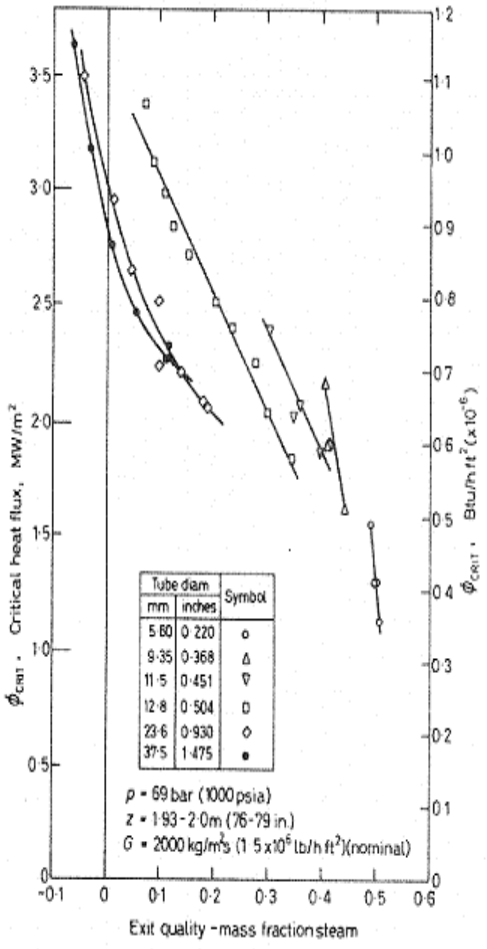

Fig. 3.3 The Influence of Tube Diameter on CHF at Fixed Exit Conditions [30].

3.3 Empirical Correlation of Experimental Data

As evident from equation 3.6 and 3.7 CHF correlations may be divided into two main groups:

3.3.1 *Local conditions – type CHF correlations* where CHF = $fn(G, x(z), p, D, z)$. These correlations are convenient to use for predicting the location of burnout and magnitude of CHF.

3.3.2 *Global conditions correlations* where burnout power = $fn(G, i(z), p, D, z)$. These correlations predict only burnout power. They cannot be used to predict the location of burn out or the magnitude of the CHF.

Probably the most general of the empirical correlations suggested to date that fall in the first category is that by Macbeth [20] based on hypothesis proposed and tested by Barnett [21]. This hypothesis, the 'local conditions hypothesis' suggests that the critical heat flux is solely a function of the mass quality at the point of overheating, as suggested by equation (3.11). Barnett and Macbeth make a further simplifying assumption that the critical heat flux is a linear function of quality, thus:

$$\phi_{crit} = A - B\,x(z) \tag{3.14}$$

where A and B are assumed to be function of G, p, and D. Substituting for x(z) from equation (3.5)

$$\phi_{crit} = A - \frac{B}{i_{fg}}\left[\frac{4\phi_{crit}\,z}{DG} - (\Delta i_{sub})_i\right] \tag{3.15}$$

rearranging and substituting C = 4 B/i_{fg} D G

$$\phi_{crit} = \frac{A + CDG(\Delta i_{sub})_i / 4}{1 + Cz} \tag{3.16}$$

and

$$\phi_{crit} = A - CDGi_{fg}\,x(z)/4 \tag{3.17}$$

Earlier work by Macbeth [22] had suggested that it was desirable to divide the critical heat flux data into two regions depending upon the particular values of the independent variables. Referring to the plot of critical heat flux versus inlet subcooling (Figure 3.2) it is noted that the individual lines extrapolate to definite intercepts at zero inlet subcooling ($(\Delta i_{sub})_i = 0$). This value of critical heat flux Macbeth termed the 'basic burnout heat flux' ϕ_o. Plot of ϕ_o against mass velocity showed a number of general characteristics (Figure 3.4).

At low mass velocity ϕ_o is almost directly proportional to mass velocity G. The region over which this proportionality applies is called the 'low mass velocity region'. At high mass velocities ϕ_o is relatively insensitive to mass velocity- this zone is known as the 'high mass velocity region'. The two regions are joined by a smooth continuous transition. The units of heat flux are [Btu/h.ft^2], of mass velocity [lb/h.ft^2], of enthalpy [Btu/lb], of length and diameter [inches], and of pressure [psia]. Macbeth examined the

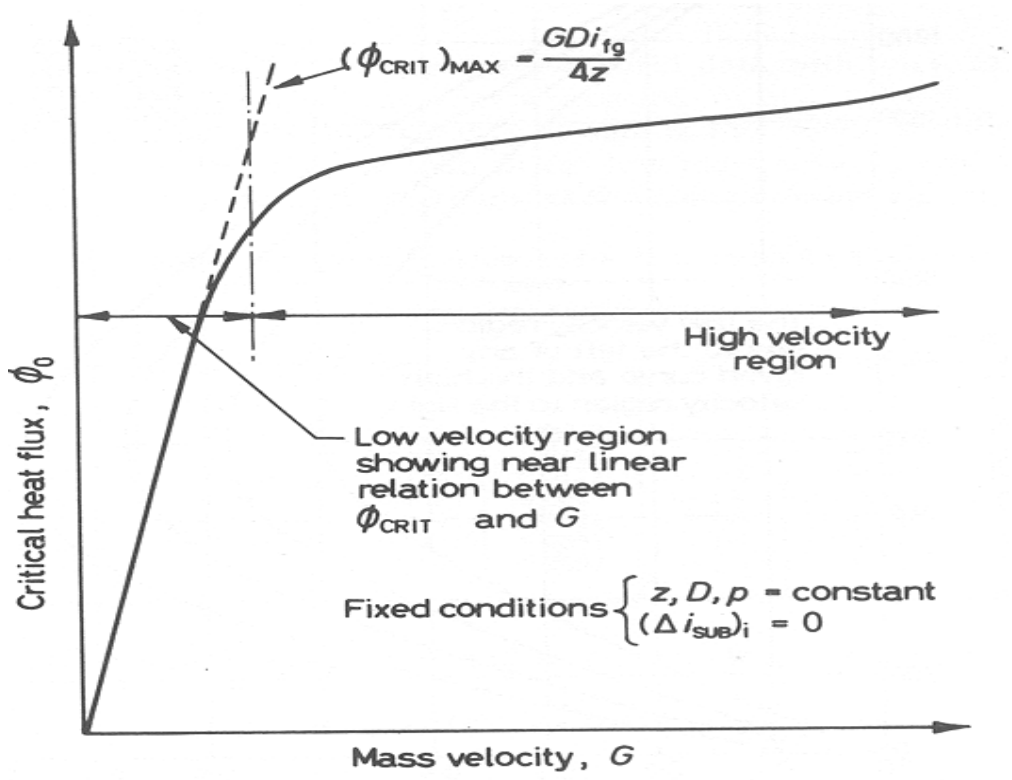

Fig 3.4 Variation of 'Basic Burnout Heat Flux' With Mass Velocity [30].

available world data in two groups, corresponding to the low and high mass velocity regions:

1. The low mass velocity region. Macbeth assumed that for a given pressure, A and C in equation (3.16) were simple power functions of G and D, viz.,

$$A = y_o D^{y1} G^{y2} \tag{3.18}$$

and

$$C = y_3 D^{y4} G^{y5} \tag{3.19}$$

the values of the constants y_o to y_5 were optimized using a computer.

Thus

$$(\phi_{crit} * 10^{-6}) = \frac{A_1 + C_1 D(G * 10^{-6})(\Delta i_{sub})_i / 4}{1 + C_1 z} \tag{3.20}$$

where

$$A_1 = 0.00106 i_{fg} D^{-0.63} (G * 10^{-6})^{-0.17} \tag{3.21}$$

and

$$C_1 = 0.00344 D^{-1.73} (G * 10^{-6})^{-1.22} \tag{3.22}$$

A simplification can be obtained by considering the limiting condition

$\phi_{crit} \rightarrow 0$, $x(z) \rightarrow 1$ (Fig. 3.4) and $A = C\ D\ G\ i_{fg} / 4$

This simplification leads to

$$(\phi_{crit} * 10^{-6}) = \frac{(G * 10^{-6})\left(i_{fg} + (\Delta i_{sub})_i\right)}{135(G * 10^{-6})^{0.5} + 4z / D} \tag{3.23}$$

or

$$(\phi_{crit} * 10^{-6}) = \frac{i_{fg}}{135}(G * 10^{-6})^{0.5}\left(1 - x(z)\right) \tag{3.24}$$

Equation (3.23) and (3.24) fit the appropriate world data with an R. M. S. error of 5.5 percent and are applicable to any system pressure.

2. The high mass velocity region. Analysis of data in this region is difficult because the pressure effect is more complex than in the low mass velocity region. Macbeth divided up the data into a number of groups, each having a nominal system pressure. The data in each pressure group were used to find the form of the power functions thus

$$A_1 = y_0 D^{y1} (G * 10^{-6})^{y2} \tag{3.25}$$

and

$$C_1 = y_3 D^{y4} (G * 10^{-6})^{y5} \tag{3.26}$$

Table 3.1 Macbeth correlation – optimized 'y' values and R.M.S. errors for high velocity critical heat flux regions [30].

Pressure psia	y_0	y_1	y_2	y_3	y_4	y_5	R.M.S. error %	No. of data points
15	1·12	−0·211	0·324	0·0010	−1·4	−1·05	13·8	88
250 (nom)	1·77	−0·553	−0·260	0·0166	−1·4	−0·937	4·7	237
530 (nom)	1·57	−0·566	−0·329	0·0127	−1·4	−0·737	5·7	170
1000	1·06	−0·487	−0·179	0·0085	−1·4	−0·555	7·4	405
1570 (nom)	0·720	−0·527	0·024	0·0121	−1·4	−0·096	3·4	133
2000	0·627	−0·268	0·192	0·0093	−1·4	−0·343	9·0	362
2700 (nom)	0·0124	−1·45	0·489	0·0097	−1·4	−0·529	4·7	37

Computer optimized values of y_o to y_5 for each pressure group are given in table 3.1. In later work Thomson and Macbeth [23] found that simple power functions for a and C were not satisfactory over the very wide range of parameters now present in the listed world data. A more complex function was required and restricted form of polynomial was used. The revised equation is of the general form

$$(\phi_{crit} * 10^{-6}) = \frac{A^1 + D(G * 10^{-6})(\Delta i_{sub})_i}{C^1 + z} \tag{3.27}$$

or written in terms of the exit steam quality x(z)

$$(\phi_{crit} * 10^{-6}) = \frac{A^1 - D(G * 10^{-6}) i_{fg} x(z)/4}{C^1} \tag{3.28}$$

where

$$A^1 = Y_0 D^{Y1} (G * 10^{-6})^{Y2} \left[1 + Y_3 D + Y_4 (G * 10^{-6}) + Y_5 D (G * 10^{-6})\right] \tag{3.29}$$

and

$$C^1 = Y_6 D^{Y7} (G * 10^{-6})^{Y8} \left[1 + Y_9 D + Y_{10} (G * 10^{-6}) + Y_{11} D (G * 10^{-6})\right] \tag{3.30}$$

The new constants Y_0 - Y_{11} are listed in table 3.2 together with the number of experiments and the R. M. S. error for each group.

Biasi et al. [24] also proposed correlation for determining critical heat flux which has an advantage of being continuous with respect to 'system pressure' with apparently little or no loss of accuracy.

$$\phi_{crit} = \frac{1.883 * 10^3}{D^n G^{1/6}} \left[\frac{f(p)}{G^{1/6}} - x(z)\right] \tag{3.31}$$

for the low quality region

$$\phi_{crit} = \frac{1.78 * 10^3 h(p)}{D^n G^{0.6}} \left[1 - x(z)\right] \tag{3.32}$$

for the high quality region

Where n = 0.4 for D ≥ 1 cm

n = 0.6 for D < 1 cm

and $f(p)$ = 0.7249 + 0.099p exp(-0.032p)

$$h(p) = -1.159 + 0.149 p \exp(-0.019 p) + \frac{8.99 p}{10 + p^2}$$

The correlation is evaluated in c.g.s. units, i.e., ϕ_{crit} in W/cm^2 and is valid over the following range of variables.

0.3 cm < D < 3.75 cm.

20 cm < z < 600 cm.

2.7 bar < p < 140 bar

10 g/cm^2 s < G < 600 g/cm^2 s

$1/(1 + \rho_l/\rho_g) < x(z) < 1$

Table 3.2 Modified constants and R.M.S. errors for Macbeth's correlation of critical heat flux, for uniformly heated vertical tubes cooled by water [30].

Constant	System pressure, psia					
	560	1000	1250	1550	1800	2000
Y_0	237	114	93·3	58·0	194	65·5
Y_1	1·20	0·811	1·10	0·834	2·09	1·19
Y_2	0·425	0·221	0·575	0·224	0·593	0·376
Y_3	−0·940	−0·128	0	−0·0336	−0·597	−0·577
Y_4	−0·0324	0·0274	0	0·0755	−0·131	0·220
Y_5	0·111	−0·0667	0	−0·296	−0·0482	−0·373
Y_6	19·3	127	88·5	48·3	231	17·1
Y_7	0·959	1·32	1·46	0·823	1·93	1·18
Y_8	0·831	0·411	1·00	0·121	0·612	−0·456
Y_9	2·61	−0·274	0	0	−0·575	−1·53
Y_{10}	−0·0578	−0·0397	0	0	−0·255	2·75
Y_{11}	0·124	−0·0221	0	0	0·110	2·24
R.M.S. error %	7·27	6·48	5·12	6·02	3·93	7·56
No. of expts.	225	802	100	527	195	615

The critical heat flux is given as the higher of the two valves obtained by the intersection of equations. (3.31) and (3.32) with the heat balance equation (3.5). For values of G below 30 g/cm^2 s eq. (3.32) is always used. The R.M.S. error for over 4500 data points examined was 7.26 per cent and 85.5 per cent of all points were correlated within ± 10 per cent.

In this section, it is seen that there are many possible ways to express CHF in terms of independent variables and, this happened worldwide so large number of correlations, similar to Macbeth and Barnett were developed, some of them are presented in Appendix A. Each correlation is presented with its critical comment.

From these correlations it is clear that these are applicable to particular conditions. So it is envisioned to have some more general approaches. Next chapter is devoted to such techniques.

CHAPTER 4

Alternative approaches to CHF

4.1 Introduction

As envisioned in previous chapter it is thrust of present technology to develop more general approach. In this chapter some of them are presented at brief.

4.2 Analytical Methods

Several analytical approaches to predict the CHF have been developed. Two popular models are those by Hewitt and Hall-Taylor [25] and Tong [26]. Hewitt and Hall-Taylor's model is a three fluid model (vapor, liquid film, entrained droplets). It is based on the commonly accepted hypothesis that the boiling crisis in annular flow occurs when the liquid film is depleted by evaporation and entrainment. Many variations of this model may be found in literature e. g. for annuli, for rod bundle and for transient conditions. Tong [26] developed a two-fluid model for the prediction of CHF in the bubbly flow regime. This model has been successfully used to include the effect of upstream axial flux distribution. All these models are basically valid for one flow regime and heat transfer configuration.

4.3 Table Look-Up Technique

Since most empirical correlations and analytical models have a limited range of application, the need for more general technique is obvious. Attempts have been made in the USSR to construct a standard table of CHF values for a given geometry (Doroshchuk et al. , [27]). An updated version of the look-up table for critical heat flux (CHFI has been developed jointly by AECL Research (Canada) and IPPE (Obninsk, Russia) [28]. It is based on an extensive data base of CHF values obtained in tubes with a vertical upward flow of steam-water mixture. While the data base covers a wide range of flow conditions, the look-up table is designed to provide CHF values for 8 mm tubes at discrete values of pressure, mass flux and dryout quality covering the ranges 0.1 to 20.0 MPa. (0.0 to 8.0 Mg m^2 s^{-1} and - 0 . 5 to +1.0 respectively. Linear interpolation is used to determine the CHF for conditions between the tabulated values, and an empirical correction factor is introduced to extend this CHF table to tubes of diameter values other than 8 mm. Compared against the combined AECL- IPPE world data bank {consisting of 22 946 data

points after excluding duplicate data and obviously erroneous data), the 1995 look-up table predicts the data with overall average and root-mean-square errors of 0.69% and 7.82% respectively. An assessment of various CHF tables and several empirical correlations shows that the 1995 table consistently provides the best prediction accuracy and is applicable to the widest range of conditions.

Table look-up techniques are accurate, simple to use, and can easily be given the correct parametric and asymptotic trends. They do not require extrapolations since the range of conditions is sufficiently wide. They do, however, require interpolation to evaluate CHF at nonmatrix conditions.

4.4 Graphical Techniques

A number of graphical techniques for predicting CHF have been developed by Katto and Shah. Katto's [29] method is based in distinguishing between various flow regimes. For each flow regime, graphs were presented to find the CHF as a function of flow and fluid properties. These graphic techniques are valid for a wide range of fluids. They are considered excellent for handbook applications and for obtaining a first estimate of the CHF value, especially for fluids for which no CHF data are available.

4.5 Subchannel Analysis

All above methods are used for tubes but in actual practice such high heat flux occurs in reactors. And in reactors rod bundle has different configuration than tubes. Also it is clear that CHF is local phenomena and to heat flux should be determined locally so now a days, method used is subchannel analysis. There are two approaches to the definition of this subchannel volume: the coolant centered and the rod centered subchannel as shown in Figure 4.1. Traditional approach for rod bundle has been coolant-centered subchannels. From now onwards only this approach will be discussed.

4.5.1 *Control Volume Selection*

The actual subchannel control volume encompasses only the coolant, not the fuel rod. It is illustrated in Figure 4.2 (a, b). However, the control volume of Figure 4.2 is used only for mass, axial momentum, and energy conservation balances. For the transverse momentum balance, a separate control volume between adjacent subchannel is employed.

4.5.2 *Continuity Equation*

From the Figure 4.3 by mass balance, it can be shown for single phase flow

$$A_{fi}\frac{\partial}{\partial t}\langle \rho_i \rangle + \frac{\Delta \dot{m}_i}{\Delta z} = -\sum_{j=1}^{J} W_{ij} \tag{4.1}$$

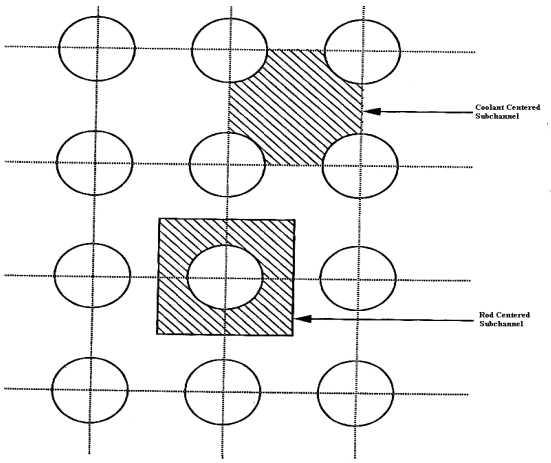

Fig. 4.1 Options for subchannel definition [31].

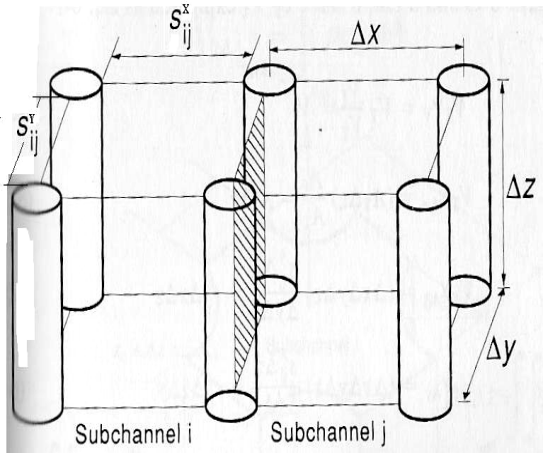

Fig. 4.2(a) Subchannel control volume (Rectangular) [31].

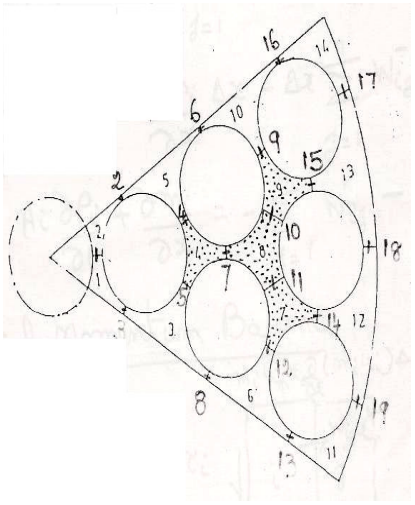

Fig. 4.2(b) Subchannal control Volume (round).

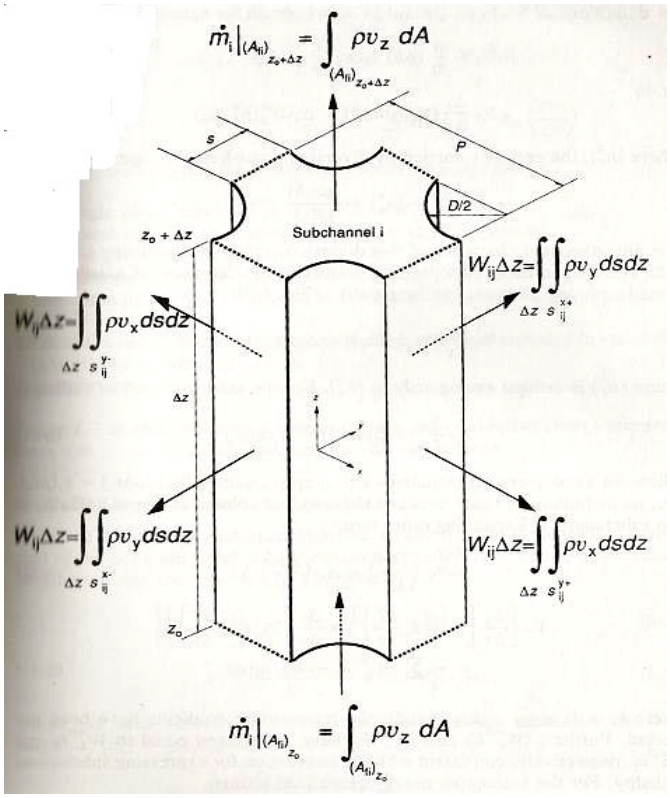

Fig. 4.3 Subchannel control volume for continuity [31].

4.5.3 *Energy equation*

By considering Figure 4.4 from energy balance it can be shown that for single phase flow

$$A_{fi}\frac{\partial}{\partial t}\langle \rho h\rangle_i + \frac{\Delta}{\Delta z}\left[\dot{m}_i\, h_i\right] = A_{fi}\left\langle \frac{Dp_i}{Dt}\right\rangle + \langle q_i'\rangle_{rb} - \sum_{j=1}^{J} W_{ij}^{*H}[h_i - h_j] - \sum_{j=1}^{J} W_{ij}\{h^*\} \qquad (4.2)$$

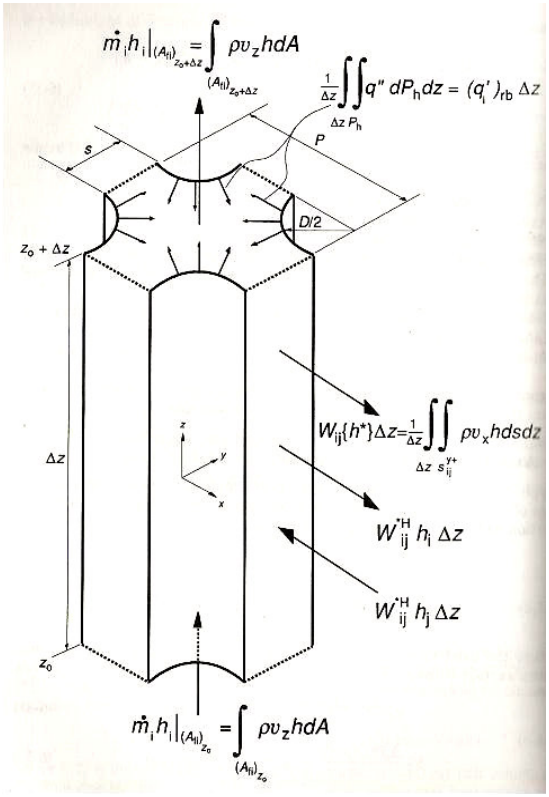

Fig. 4.4 Subchannel control volume for Energy balance [31].

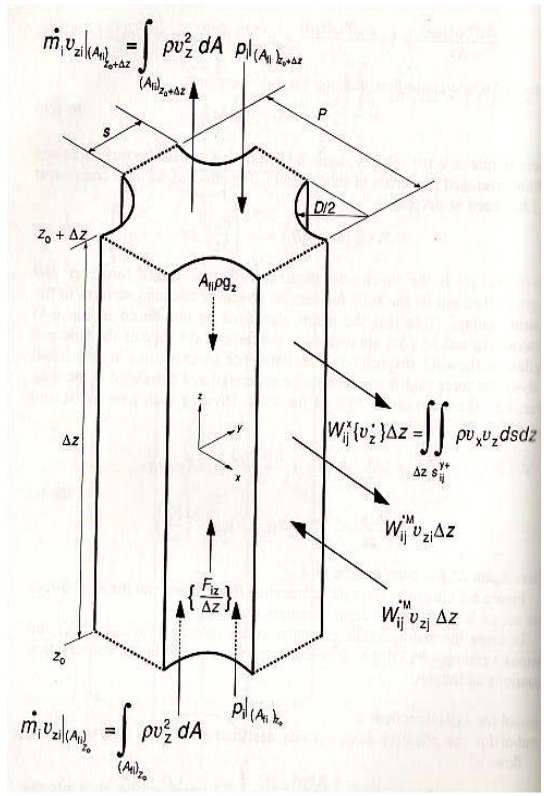

Fig. 4.5 Subchannel control volume for axial momentum balance [31].

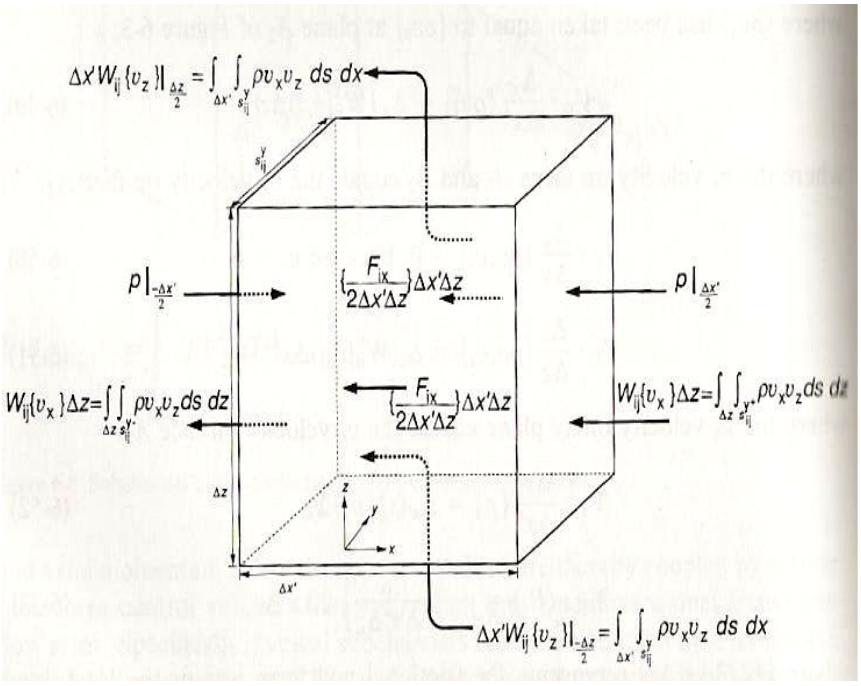

Fig. 4.6 Subchannel control volume for transverse momentum [31].

4.5.4 *Axial Linear Momentum Equation (z-direction)*

Applying the same procedure to those used in derivation of the continuity and energy equations by considering momentum conservation at Figure 4.5 it can be shown

$$\frac{\partial}{\partial t}\left\langle \dot{m}_i \right\rangle + \sum_{j=1}^{J} W_{ij}\left\{v_z^*\right\} + \frac{\Delta(\dot{m}_i\, v_{zi})}{\Delta z} = -A_{fi}\left\langle \rho \right\rangle g_z - A_{fi}\frac{\Delta\{p\}}{\Delta z} - \sum_{j=1}^{J} W_{ij}^{*M}(v_{zi} - v_{zj}) - \left\{\frac{F_{ij}}{\Delta z}\right\} \quad (4.3)$$

4.5.5 *Transverse Momentum Equation (x-direction)*

In this case now we have to change our control volume to as shown in Figure 4.6. With simple considerations it can be shown that

$$\frac{\partial}{\partial t}(W_{ij}) + \frac{\Delta}{\Delta x'}(W_{ij}\{v_x\}) + \frac{\Delta}{\Delta z}(W_{ij}\{v_z\}) = -(s_{ij}^{y}\frac{\Delta}{\Delta x'}\{p\}) - \left\{\frac{F_{ix}}{\Delta x' \Delta z}\right\} \quad (4.4)$$

It is important to note in all these four equations that W is mass/length time.

Since the introduction of numerical subchannel analysis methods in the 1960s, a great number of computer tools have been developed for utilizing this approach. Typical example of one such method is, conservation equations for Pressurized water reactor, the COBRA family.

Conclusions

The lack of success in developing realistic analytical models for the various boiling modes (with the exception of the CHF in annular flow, and liquid dispersed film boiling) has limited the full utilization of the two- and three-fluid model features of current advanced reactor safety codes.

Most heat transfer correlations are based on tube data. Extrapolation of tube correlation to bundle geometries equipped with flow obstructing spacers should not be practice in reactor safety. More generalized approach is by subchannel analysis.

No single CHF correlations can ever be expected to have a very wide range of applications since the mechanisms governing the boiling crisis change with the flow regime. The alternative approach can be CHF table look up technique. The most promising approach is by subchannel analysis.

Most heat transfer correlations are functions only of the fluid properties. Surface effects are usually ignored. The minimum film boiling temperature, however, can be strongly affected by the presence of a surface oxide layer.

REFERENCES

[1]. Volmer, M., "Kinetic der Phasenbildung," in *Die Chemische Reaktion.* Vol. 4, edited by K. F. Bonnhoeffer, Leipzig, Steinkopf (1939).

[2]. Gaertner, R. F., "Distribution of Active Sites in the Nucleate Boiling of Liquids," *A.I.Ch.E. Preprint 5,* Fifth National Heat Transfer Conference, Houston (1962).

[3]. Ellion, M. E., "A study of the Mechanism of Boiling Heat Transfer," Jet Propulsion Laboratory Memo 20-88, C.I.T. (1954).

[4]. Rohsenow, W. M., and P. Griffith, "Correlation of Maximum Heat Transfer Data for Boiling of Saturated Liquids," *Chem. Eng. Progr., Symp. Ser.* 52, No. 18, 41 (1956).

[5]. Zuber, N., "Hydrodynamic Aspects of Boiling Heat Transfer," *USAEC Report AECU*-4439 (1959). (Ph.D. Thesis, University of California, Los Angeles, 1959).

[6]. Addoms, J. N., "Heat Transfer at High Rates to Water Boiling Outside Cylinders," D.Sc. Thesis, Massachusetts Institute of Technology (1948).

[7]. Chang, Y. P., and N. W. Snyder, "Heat transfer in Saturated Boiling," *Chem. Eng. Progr., Symp. Ser.* 56, No. 30, 25-38 (1960).

[8]. Kutateladze, S. S., "Heat Transfer in Condensation and Boiling," *USAEC Report AEC-tr*-3770 (1952).

[9]. Zuber, N., M. Tribus, and J. W. Westwater, "The Hydrodynamic Crisis in Pool Boiling of Saturated and Subcooled Liquids," pp. 230-236 in *International Development in Heat Transfer, Pt. II, ASME* (1961).

[10]. Kutateladze, S. S., and L. L. Schneiderman, "Experimental Study of Influence of Temperature of Liquid on Change in Rate," pp. 95-100 in "Problems of Heat Transfer during a Change of State," *USAEC Report AEC-tr*-3405 (1953).

[11]. Ivey, H. J., and D. J. Morris, "On the Relevance of the Vapor-Liquid Exchange Mechanism for Subcooled Boiling Heat Transfer at High Pressure," *U. K. report AEEW-R-137*, Winfrith (1962).

[12]. Adams, J. M., "A Study of the Critical Heat Flux in an Accelerating Pool Boiling System," NSF G- 19697, University of Washington (1962).

[13]. Pramuk, F. S., and J. W. Westwater, *Chem. Eng. Progr. Symp. Ser.* 52, No. 18, 79 (1956).

[14]. Berenson, P. J. "Experiments on Pool-Boiling Heat Transfer," *Intern. J. Heat Mass Transfer* 5, 985 (1962).

[15]. Ivey, H. J. and D. J. Morris, "The Effect of Test Section Parameters on Saturation Pool Boiling Burnout at Atmospheric Pressure," *A.I.Ch.E. Preprint* 160, Chicago (1962).

[16]. Van Stralen, S. J. D., "Heat Transfer in Boiling Binary Liquid Mixtures at Atmospheric and Subatmospheric Pressures," *Chem. Eng. Sci.* 5, 290, 296 (1956).

[17]. Castello, C. P., and W. J. Frea, "A Salient Non-hydrodynamic Effect on Pool Boiling Burnout of Small Semi-Cylindrical Heaters," *A.I.Ch.E. Preprint* 15, Sixth National Heat Transfer Conference, Boston (1963).

[18]. Yang, Wen-Jei, "Bubble Dynamics and Nucleate Boiling Heat Transfer in Boiling Liquid Mixtures," *ASME Paper* 63-WA-19 (1963).

[19]. Lee, D. H. and Obertelli, J. D., "An Experimental Investigation of forced convection boiling in high pressure water," *Pt. I. AEEW-R* 213 (1963).

[20]. Macbeth, R. V., "Burn-out Analysis", Part 4, "Application of local condition hypothesis to world data for uniformly heated round tubes and rectangular channels," *AEEW-R* 267 (1963).

[21]. Barnett, P. G., "An investigation into the validity of certain hypothesis implied by various burnout correlations," *AEEW-R* 214 (1963).

[22]. Macbeth, R. V., "Burn-out Analysis", Part 3, "The low velocity burnout regime," *AEEW-R* 222 (1963).

[23]. Thompson, B. and Macbeth, R. V., "Boling water heat transfer – burnout in uniformly heated round tubes : A compilation of world data with accurate correlations," *AEEW-R* 356 (1964).

[24]. L. Biasi *et al.*, "Studies on burnout", Part 3, *Energia Nucleare,* 14, (9), 530-536 (1967).

[25]. Hewitt, G. F., and N. S. Hall –Taylor, "Annular Two Phase Flow," Oxford: Pergamon (1970).

[26]. Tong, L. S., "Boiling Heat Transfer and Two Phase Flow," New York: Wiley (1965).

[27]. Doroshchuk, V. E., L. L. Levitan, and F. P. Lantzman, "Investigation into Burnout in Uniformly Heated Tubes," *ASME* 75-WA/HT-22 (1975).

[28]. Groeneveld, D.C., L.K.H. Leunff, P.L. Kirillov, V.P. Bobkov, I.P. Smogalev, V.N. Vinogradov, X.C. Huang , and E. Royer, "The 1995 look-up table for critical heat flux in tubes," Nuclear Engineering and Design 163, 1-23 (1996).

[29]. Katto, Y. "A Generalized Correlation of Critical Heat Flux for the Forced Convection Boiling in Vertical Uniformly Heated Round tubes," *Int. J. Heat Mass Transfer* vol. 21, pp. 1527-1542 (1978).

[30]. Collier, J. G., "Convective Boiling and Condensation," Second Edition London: McGraw-Hill (1980).

[31]. Todreas, N. E., M. S. Kazimi, "Nuclear Systems II – Elements of Thermal Hydraulic Design," New York: Hemisphere Publishing Corporation, 1990.

[32]. Hewitt, G. F., J. M. Delhaye, N. Zuber, "Multiphase Science and Technology," vol. 2, New York: Hemisphere Publishing Corporation, 1986.

[33]. Griffiths, P., J. F. Pearson, and R. J. Lepkowski, "Critical Heat Flux during a Loss – of – Coolant Accident," *Nucl. Saf.* Vol. 18, no. 3, pp. 298-305 (1977).

[34]. Gellerstedt, J. S., R. A. Lee, W. J. Oberjohn, R. H. Wilson, and L. J. Stanek, "Correlation of Critical Heat Flux in a Bundle Cooled by Pressurized Water," "Two-Phase Flow and Heat Transfer in Rod Bundles," ASME Winter Annual Meeting, Los Angeles, pp. 63-71 (1969).

[35]. Levitan, L. L., and F. P. Lantsman, Critical Heat Flux in Internally Heated Annular Channels, *Therm. Eng. (USSR)* vol. 24, no. 4, pp. 16-21 (1977).

APPENDIX A

CHF Correlations

1. Mecbeth [20]. Only for low –flow tube CHF. Upper mass flux boundary depends on pressure and is defined graphically in original reference.

$$CHF = \frac{8.585 H_{fg} (G/1356)^{0.51} (1-x)}{1.444 Dhy^{0.1}}$$

2. Doroshchuk et al .[27]. Based on large number of tube data obtained at :
P: 2900-15, 600 kPa, $T_{sub} < 50^{o}$ C, G < 2000 kg/m^{2}s, D: 0.004-0.016m

$$CHF = 10^3 \left[10.3 - 17.5 \frac{p}{p_{cr}} + 8.0 \left(\frac{p}{p_{cr}} \right)^2 \right] \left(\frac{G}{1000} \right)^a \left(\frac{0.008}{d} \right)^{1/2} e^{-1.5X}$$

Where $a = 0.68 \frac{P}{P_{cr}} - 1.2X - 0.3$

3. Zuber –Griffith correlation [33]. Recommended for G < 300 kg/m^{2}s and up or downflow. Under predicts CHF at high α-values.

$$CHF = (1-\alpha) 0.131 \rho_g H_{fg} \left[\frac{\sigma g (\rho_f - \rho_g)}{\rho_g^{\,2}} \right]^{0.25}$$

4. B&W-2 correlation [34]. Based on 207 bundle CHF data. Date base range:
P: 13,800 – 16,550 kPa, G: 1020 – 5424 kg/m^{2}s, X: -0.03 - +0.20

$$CHF = \frac{1.155 - 16.03 Dhy}{4.03x10^3 \left(2.25x10^{-3} G \right)^A} \left[3.7x10^7 \left(4.36x10^{-4} G \right)^B - 48.22 x H_{fg} G \right]$$

Where A = 0.712 + 3 x 10^{-5} (P-13,790)

B = 0.834 + 9.9 x 10^{-5} (P-13,790)

5. Levitan and Lantsman correlation [35]. Based on large number (>>1000) of annuli data obtained at: L: 0.5, D: 0.006-0.1 m, Dhy: 0.002-0.006 m, P: 5000-20,000 kPa, G: 250-5000 kg/m^{2}s, x < 0.3

$$CHF = 0.18 CHF_{PB} G^{0.25} \left(1 - \frac{P}{P_{cr}} \right)^{0.1} \left(\frac{Dhy}{D_i} \right)^{0.2} \left[1 - 0.06 G^{0.5} \left(\frac{Dhy}{D_i} \right)^{0.2} x \right]$$

Where $CHF_{PB} = 0.14\ H_{fg}\ \rho_g^{0.5} [\sigma g(\rho_l - \rho_g)]^{0.25}$

ACKNOWLEDGEMENT

Technology is like an ocean and engineer is like a pearl diver in search of treasure beneath the sea. There is no end to the technical studies but an engineer try to get as much as possible.

This is to acknowledge my indebtedness to my guide **Prof. Kannan N. Iyer**, Department of Mechanical Engineering, IIT Bombay for his guidance and suggestions for preparing this seminar report. His towering presence instilled in me the craving to work harder and complete this daunting task timely with a sufficient degree of independent study. All though he has helped me encouragingly to metamorphosis this seminar and give it the shape that it has got.

I also wish to thank our institute librarian and to fellow students of my class for being kind enough to get useful suggestions and further cooperation.

Sandeep Chittora